

# Effect of the electric field on the form stability of a Schottky electron emitter: A step model

M. S. Bronsgeest<sup>a)</sup> and P. Kruit

Delft University of Technology, Lorentzweg 1, 2628 CJ Delft, The Netherlands

(Received 24 June 2008; accepted 29 September 2008; published 1 December 2008)

The stability of the physical shape of an electron emitter (co)determines the stability of the performance of electron-beam equipment. A typical short-term instability of the Schottky electron source is the instability of the (100) facet at the tip end known as “collapsing rings.” This instability causes probe instabilities, but it is known from experiments that this can be prevented by applying high enough extraction voltages. The phenomenon of collapsing rings can be explained with a step-flow model, which is based on variations in equilibrium concentrations of adatoms on the surface. The effect of the extraction voltage can be incorporated by acknowledging the redistribution of the surface charge associated with adatom formation. For operation at constant extraction voltages the adatom formation energy becomes a function of the local charge density. The charge-density distribution on the emitter surface as a function of the applied extraction voltage can be calculated with boundary-element methods. It is shown that, provided the relevant material properties are known, it can be predicted if, for a given tip shape, a collapse is to be expected.

© 2008 American Vacuum Society. [DOI: 10.1116/1.3010732]

## I. INTRODUCTION

The ultimate performance of today’s focused electron-beam equipment is largely determined by the source quality. Preferably, the source quality remains high over a long time period (months to years), and for some applications the short-term stability (hours) is also relevant. A key factor in both long- and short-term stabilities is the stability of the physical shape of the source. The emitter shape is generally not a thermodynamic equilibrium. As a consequence, source types that are operated at elevated temperatures can evolve and display a performance that is not constant in time. A common emitter type in focused electron-beam equipment is the Zr/O/W(100) Schottky emitter,<sup>1</sup> which normally operates at 1800 K and at extraction fields of  $\sim \frac{1}{2} - 1$  V/nm.

A typical short-term instability of the Schottky source is the instability of the (100) facet at the tip end ( $\sim 0.3 \mu\text{m}$   $\varnothing$ ) known as “collapsing rings,”<sup>2</sup> which develop when operating the source at relatively low extraction voltages.

Collapsing rings were first discovered in 1955 in the emission patterns of heated W(110) emitters in pulsed field mode<sup>2</sup> and were associated with a redistribution of material, making the emitter slightly thicker and shorter. Theory was developed that predicted the shortening rate as a function of field strength,<sup>3</sup> but this theory does not explain the formation of rings.

Over the past decade, the interest in the stability of nanostructures has increased, and collapsing rings can now be recognized as a decay mechanism that can be adequately described with step-flow models.<sup>4</sup> The basic step model, however, does not include the effect of the extraction voltage. Giesen *et al.*<sup>5</sup> expanded the step model by including the effect of applying a potential to the surface assuming the

potential generates a uniform electric field. This applies to experimental studies on nanostructures on metal surfaces submerged in electrolyte, in which the electrical double layer that forms on the surface ensures a uniform charge density and electric field. The electric field on an operating Schottky emitter, however, is not uniform. In this work, we incorporate this in the step model. Provided the material properties are known, this enables us to describe both the phenomenon of collapsing rings and their response to an extraction voltage.

First we will introduce the Schottky emitter and its collapsing rings in somewhat more detail (Secs. II and III), and we will give the more historic equation that predicts that an emitter will stop receding (through collapsing rings) when the extraction voltage is high enough (Sec. IV). Then, we will give the basic assumptions of the step-flow model as set up by Israeli and Kandel,<sup>4</sup> which can explain the phenomenon of the collapsing rings (Sec. V). To explain why the collapsing rings will stop at high enough extraction voltages within the step model, we use the theory developed by Giesen *et al.*,<sup>5</sup> which we will introduce in Sec. VI. Finally, we will apply the model to emitters, and we will show in Sec. VII that depending on the emitter geometry, the model predicts that an extraction voltage can indeed prevent the occurrence of collapsing rings.

## II. SCHOTTKY EMITTER

Figure 1 shows a scanning electron microscope (SEM) image of a Zr/O/W(100) emitter in full length and also a close-up of the tip end. The emitter is made of a single-crystalline tungsten wire with the (100) planes perpendicular to the wire axis. One end is etched to a small radius tip of usually  $0.3 - 0.8 \mu\text{m}$ ; the other end is attached to a heating filament. About halfway along the wire is a reservoir con-

<sup>a)</sup>Electronic mail: m.s.bronsgeest@tudelft.nl

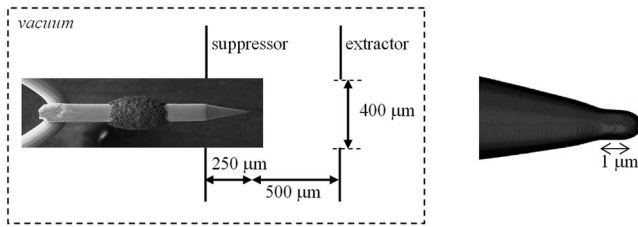


FIG. 1. SEM image of a Schottky electron emitter in the schematic gun geometry. On the right is a close-up of the tip end.

taining  $ZrO_x$ . At elevated temperatures, the  $ZrO_x$  diffuses across the surface toward the tip end and reduces the work function of the (100) planes to 2.9 eV. The typical operating temperature is 1800 K. The emitter is placed in a gun with a suppressor and an extractor, as shown in Fig. 1. The suppressor is biased negatively with respect to the emitter to suppress emission from the shanks, whereas the extractor is biased positively to extract the electrons from the tip. For the standard gun geometry as given in Fig. 1, the suppressor voltage is  $-300$  V and the extraction voltage is  $\sim 3-7$  kV depending on the emitter radius and the desired beam properties.

### III. PROBE INSTABILITIES DUE TO COLLAPSING RINGS

The part of the Schottky emitter surface that emits the probe current is the facet at the tip end. The total current emitted by the facet is typically tens of microamperes. The final probe used in practical applications contains a small percentage of this: typically a few picoamperes up to  $\sim 100$  nA. When the emitter is operated at low extraction voltages, the facet can become unstable. This gives typical probe instabilities as illustrated in Fig. 2.

The probe instabilities are caused by geometrical instability of the facet. This instability is historically known as collapsing rings<sup>2</sup> because they were observed in the electron emission pattern as contracting bright rings. Schottky emitters frozen in the middle of such an instability show islands on the facet with a height of up to tens of nanometers (Fig. 3).

We have investigated collapsing rings on Schottky emitters and the exact relation with the typical probe instabilities

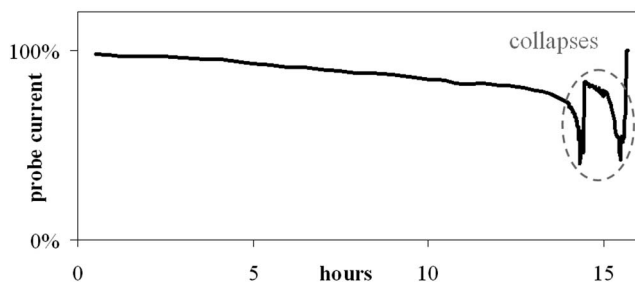


FIG. 2. Typical probe instabilities during collapsing rings on a Schottky emitter.

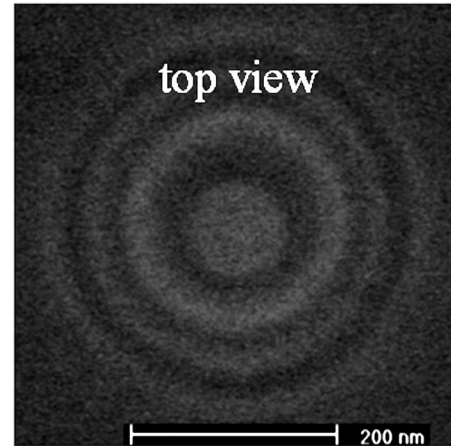
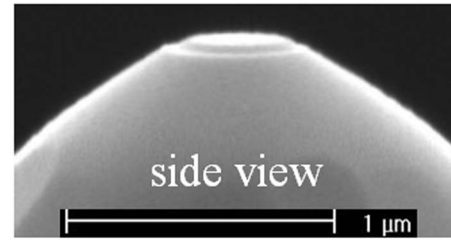


FIG. 3. Top-view and side-view SEM images of two Schottky emitters frozen in different stages of a collapse process.

and will discuss this in more detail in a future publication. Here, we focus on how we can predict theoretically the occurrence of these rings.

### IV. "RING-STOPPING" FIELD

Historically, the interest in collapsing rings came from the fact that observing collapsing rings could be used to extract material properties, such as surface diffusion parameters and surface tension.<sup>6</sup> The theory<sup>7,8</sup> behind these ring-counting experiments requires that bulk and surface are in local thermodynamic equilibrium, so that a local chemical potential can be assigned to the surface. The surface chemical potential gives the free-energy change per atom upon locally adding or removing a small volume of material, and it can be described as an analytical function of the local surface slope. Along a surface with slope variations, the associated variations in chemical potential will drive mass transport. For emitters, it is assumed that the mass transport is through surface diffusion only. Because the curvature along an emitter surface decreases on going from the apex toward the shank, the direction of net diffusion points away from the apex. As a result, the emitter will recede.

When the extraction voltage is applied, the surface chemical potential is no longer a function of the local slope alone but also of the energy density of the local electric field: the free-energy change per atom upon locally adding a small volume is reduced, with the electric-field energy stored in the vacuum volume it replaces. The electric field changes along the emitter surface and is strongest near the apex. Barbour *et al.*<sup>3</sup> concluded from field calculations for sphere-on-cone ge-

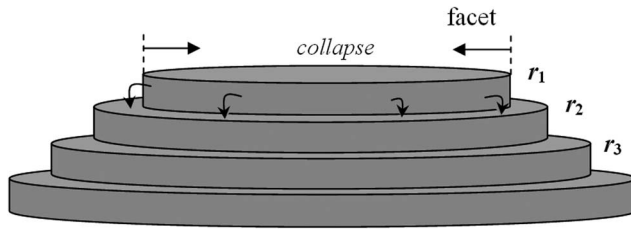


FIG. 4. Model of emitter tip end in step-flow model description: stack of concentric terraces of different radii.

ometries and inspection of emitter profiles on shadowgraphs that the ring-stopping field, being the field at the apex that will stop emitter recession, can be given by

$$E_{\text{stop}} = 2 \sqrt{\frac{\gamma/2}{\epsilon_0 r_{\text{tip}}}}, \quad (1)$$

with  $\epsilon_0$  the permittivity of vacuum. Equation (1) has been used to calculate the surface tension  $\gamma$  from the experimental stopping field and the tip radius  $r_{\text{tip}}$ . The fields were calculated from the experimental extraction voltages by approximating the emitter with a sphere-on-cone geometry. It is noted that Eq. (1) only applies to specific emitter profiles with round tip ends. Schottky emitters have a facet at the tip end. Swanson and Schwind<sup>1</sup> experimentally determined a stopping field of 0.8 V/nm for a Schottky emitter with a radius of 0.5  $\mu\text{m}$  operating at 1800 K. Here, the stopping field is the field at the facet center, which was calculated from the experimental extraction voltage and the gun geometry with a finite-difference routine in which the emitter tip end was approximated with a truncated sphere.

The theory behind Eq. (1) offers an explanation for the experimentally observed stopping of ring formation for high enough extraction voltages. However, it is a theory that treats the surface profile as a continuous function, and thus ignores the presence of steps. Therefore, it is incapable of describing the phenomenon of the rings and how the field affects them.

## V. COLLAPSING RINGS IN THE STEP-FLOW MODEL

To explain the phenomenon of collapsing rings on emitters, we follow Israeli and Kandel<sup>4</sup> and model the emitter tip end as a stack of (100) terraces bound by circular concentric steps (Fig. 4). In practice, the Schottky emitter facet can be square or octagonal, but this only occurs at higher extraction voltages where collapse does not occur. The rotationally symmetric stack is in agreement with SEM images of Schottky emitters frozen in the collapse process, such as in Fig. 3.

A collapse is the shrinking of the top terrace or the top bunch of terraces. The terrace (bunch) shrinks when its bounding step emits atoms onto the underlying terrace. These adatoms can diffuse across the surface and can be absorbed at the steps bounding the terrace. To describe the collapse, we need to look at atom transport from and to the steps. Evaporation, bulk diffusion, and formation of islands

and voids are ignored. To solve the diffusion equations, we need the equilibrium concentrations of adatoms on the terraces. The local equilibrium adatom concentration on a terrace depends on the work to create the adatom and the temperature:<sup>4</sup>

$$C^{\text{eq}} = \frac{1}{\Omega_s} e^{-U_{\text{ad}}/k_B T}, \quad (2)$$

with atomic area  $\Omega_s$ , adatom formation energy  $U_{\text{ad}}$ , the Boltzmann constant  $k_B$ , and temperature  $T$ . The adatom creation energy  $U_{\text{ad}}$  is defined as the work to bring an atom from a kink site in a step onto the terrace. The work to create an adatom depends on the local environment, such as the local curvature of the step and the local step density. Because the terraces in Fig. 4 are not equivalent, this gives rise to differences in concentrations across the stack. If temperature allows, diffusion will take place and the steps will start moving due to a net adatom absorption or emission. The equilibrium adatom concentration  $C_i^{\text{eq}}$ , near the curved step edge of terrace  $i$  with radius  $r_i$ , can be written as<sup>4</sup>

$$C_i^{\text{eq}} = \frac{1}{\Omega_s} \exp \left[ \left( -U_{\text{ad}0} + \frac{\Omega_s \beta}{r_i} + \sqrt{\Omega_s} \frac{\partial [U_{\text{int}}(r_i, r_{i+1}) + U_{\text{int}}(r_i, r_{i-1})]}{\partial r_i} \right) / k_B T \right], \quad (3)$$

with  $\beta$  the step line tension being the work per unit length to extend the step and  $U_{\text{int}}$  the interaction energy between two steps.

The  $1/r$  term gives a reduction in the work to create the adatom due to the step curvature. As a result, the equilibrium adatom concentration is larger for terraces of smaller radius. Net diffusion will take place from the small terraces toward the lower terraces, and the stack will decay.

Step-step interaction can be either attractive or repulsive, so it can either decrease or increase the work to create an adatom. There is a general consensus that the most important step interaction between steps with step separation  $\Delta r$  corresponds to a  $1/(\Delta r)^2$  interaction law,<sup>9</sup> which covers three contributions: entropic interaction due to the formation of kinks and dipole-dipole interactions due to elastic as well as electric dipoles associated with steps. The  $1/(\Delta r)^2$  interaction law for steps on a rotationally symmetric structure as in Fig. 4 can be written as<sup>10</sup>

$$U_{\text{int}}(r_i, r_{i+1}) = 2\pi g \frac{r_i r_{i+1}}{r_i + r_{i+1} (r_i - r_{i+1})^2}, \quad (4)$$

in which  $g$  is a measure of the interaction strength. For the cone-shaped stack of Fig. 4, this model gives an interaction contribution in Eq. (3) that decreases with increasing terrace radius.

The geometry of the stack yields an adatom concentration gradient, but how the system responds to this depends on how fast the adatoms diffuse across the terraces and across the steps. We can calculate the evolution of the tip end by solving the diffusion equation for adatoms on the terraces between the steps, with the appropriate boundary conditions

applied at the step edges. This gives a set of coupled equations of motion for the steps.<sup>4</sup> Usually two cases are distinguished: slow terrace diffusion and fast attachment and detachment from the steps versus fast terrace diffusion and slow attachment and detachment from the steps. With strong step-step repulsion [large  $g$  in Eq. (4)], Israeli and Kandel<sup>4</sup> predicted for both cases the successive collapse of single atomic layers, whereas for weak step-step repulsion, they showed that in the second case the steps can bunch together and collapse collectively. Then the collapses of lower terraces overtake the collapse of a higher terrace and the collapse continues as a many-layer event. Both single-layer collapse and step-bunch formation and collapse have been observed experimentally for different materials.

Single atomic-layer collapses have, e.g., been reported for W(110), Mo(110), Ta(110),<sup>11</sup> Re(10–10), Re(0001), Ro(111), Ir(111),<sup>6</sup> Pb(111),<sup>12</sup> Cu(111),<sup>13</sup> and Au(100) (Ref. 14) structures, while step-bunch formation and collapse were noticed, e.g., for W(110) and Mo(110) emitters in the presence of carbon or silicon.<sup>11</sup> It is known that adsorbates can induce step-bunch formation,<sup>15</sup> and considering the height of islands on the facet in a collapse process (Fig. 3), this also seems to be the case for the Schottky emitter, which has the  $ZrO_x$  adsorbates on the W(100) terraces. It is noted that for clean W(100) single atomic-layer collapses have been reported.<sup>6</sup>

## VI. STEP MODEL INCLUDING THE EFFECT OF AN EXTRACTION VOLTAGE

To take into account the effect of the extraction voltage, Giesen *et al.*<sup>5</sup> used a different approach than that given in Sec. IV. Here, the changes induced by applying an extraction voltage are considered on an atomistic scale. Key to this approach is the change in the local charge density at the surface upon the creation of an adatom.<sup>16</sup> The charge redistribution induced by an adatom can be characterized with a dipole moment  $p$  and it changes the work function of the surface:

$$\Delta V = \frac{Cp}{\epsilon_0}, \quad (5)$$

with  $C$  the local adatom concentration. For the emitter in operation, the work-function change means a change in the potential difference between the emitter and extractor, and thus, a change in the work the power supply has to do to bring back the extraction potential to its original value. Each adatom is thus accompanied with a compensating charge flow. The compensating work per adatom delivered by the power supply to restore the extraction potential is given by

$$-\frac{\sigma \Delta V}{C} = -\frac{\sigma p}{\epsilon_0} = -pE, \quad (6)$$

with  $\sigma$  the local charge density (negative field points away from surface). The total work to create the adatom on the surface of an emitter in operation is thus different from the work at zero extraction potential:

$$U_{ad} = U_{ad0} - pE. \quad (7)$$

A positive dipole moment would increase the work per adatom for an operating emitter; a negative dipole moment would decrease it. This means that when the extraction voltage is applied, Eq. (3) changes to

$$C_i^{eq} = \frac{1}{\Omega_s} \exp \left[ \left( -U_{ad0} + pE + \frac{\Omega_s \beta}{r_i} + \sqrt{\Omega_s} \frac{\partial [U(r_i, r_{i+1}) + U(r_i, r_{i+1})]}{\partial r_i} \right) / k_B T \right]. \quad (8)$$

Steps also have dipole moments, and the step line tension and step-step interaction will also change with the applied potential difference,<sup>17</sup> but we will neglect this.

The field dependence of the equilibrium concentration will affect the concentration on the terraces of the stack in Fig. 4. For a positive adatom dipole moment, the equilibrium adatom concentrations will decrease with increasing extraction potential (increasingly negatively charged).

Due to the geometry of the emitter, the charge density on the emitter surface is a function of position, and thus has a position-dependent contribution to the equilibrium adatom concentration. The  $pE$  term in Eq. (8) changes to  $pE(x)$ , where  $x$  is the distance along the surface measured from the facet edge. The relation between  $x$  and the step curvature  $r$  depends on the tip geometry. Decay on emitter tip ends can thus, in principle, be prevented by an electric-field gradient that balances the step-curvature term.

## VII. APPLICATION TO SCHOTTKY EMITTERS

We apply the theory above to the emitter profile shown in Fig. 5, which is a contour copied from a side-view SEM image of a Schottky source. We consider three different tip-end geometries and look at the first tens of nanometers below the facet because this is the area relevant to step bunches on Schottky emitters (Fig. 3).

The field distribution along the tips is calculated for different extraction voltages with a charge-density method.<sup>18</sup> The gun geometry is that of Fig. 1. The distance between the facet and extractor is slightly different for the different geometries (Fig. 5), but its effect on the field at the emitter surface is negligible. Figure 6 gives the calculated field strength across the emitter surface (at 6 nm distance) for an extraction voltage of 4 kV.

Figure 6 shows that the electric-field strength displays a peak near the facet edge, which increases with increasing facet diameter. This is related to the increasing contact angle with increasing facet diameter (here, for the 100 nm facet: 7°; 200 nm facet: 13°; 300 nm facet: 20°). The field at the facet center that is relevant to the probe quality decreases with increasing facet diameter. The portion relevant to ring stopping in our model is the part of the curve that starts at the facet edge. For that part, the field and the field gradient are strongest for the largest facet.

To calculate the effect of these field distributions on the equilibrium concentrations near the steps, several material

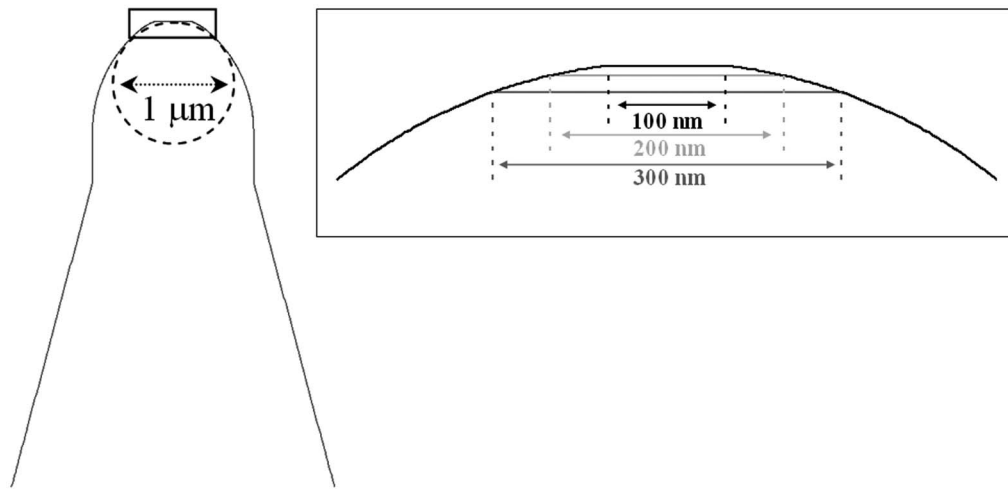


FIG. 5. Profile of the Schottky emitter used in field calculations and a close-up of the tip-end geometries investigated.

properties are required [Eq. (8)]. The atomic area of W(100) is  $1.00 \cdot 10^{-19} \text{ m}^2$ , but for the Schottky emitter, the other parameters in Eq. (8) are basically unknown. In the first approximation, we neglect step-step interaction and the effect of the extraction voltage on the step line tension. To illustrate the effect, we are mainly interested in the step-curvature term and the field term in the exponent of Eq. (8). Therefore, we rewrite Eq. (8) as

$$C^{\text{eq}}(x) = C_0 A(x) = C_0 e^{[\Omega_s \beta / r(x) + p E(z)] / k_B T}, \quad (9)$$

with  $C_0$  the equilibrium adatom concentration for a large terrace in the absence of a field [Eq. (2) with  $U_{\text{ad}} = U_{\text{ad}0}$ ], and calculate only the multiplication factor  $A(x)$ . For the multiplier  $A$ , we only need a step line tension and an adatom dipole moment. For the adatom dipole moment, we use  $0.05 \text{ e}\text{\AA}$ . This is less than the  $0.2 \text{ e}\text{\AA}$  for a tungsten adatom on the most densely packed tungsten plane (110), reported by Besocke and Wagner,<sup>19</sup> and also smaller than the  $\sim 0.1 \text{ e}\text{\AA}$

calculated by Müller and Ibach<sup>16</sup> for the (100) planes of the fcc materials Au, Cu, and Ag, which also have a higher packing density than the (100) plane of the bcc structure of tungsten. For W(110), step line tension data are available<sup>20</sup> and range from  $0.1$  to  $0.3 \text{ eV}/\text{\AA}$  depending on the step orientation. Rather arbitrarily, we use for our system the average value of  $0.2 \text{ eV}/\text{\AA}$ . The temperature is the standard operating temperature for Schottky emitters:  $1800 \text{ K}$ .

Figure 7 shows how multiplier  $A$  varies along the surface of the different tip ends in Fig. 5 in the absence of field and for the field distribution shown in Fig. 6. A larger  $A$  value means at that position a higher equilibrium adatom concentration.

At  $0 \text{ kV}$ , the equilibrium adatom concentration decreases with increasing distance from the facet edge because the terrace radius increases in going in this direction. Atom transport points away from the apex, and it is expected that the facet will collapse. The tip end with the smallest facet has the largest concentration and largest concentration gradient.

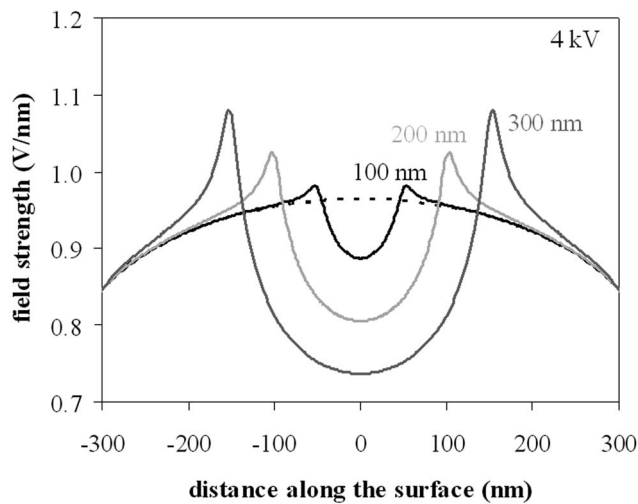


FIG. 6. Electric-field strength along the surface of a Schottky electron emitter (Fig. 5) in a standard gun module (Fig. 1) with an extraction voltage of  $4 \text{ kV}$ . Dashed line indicates field distribution without a facet.

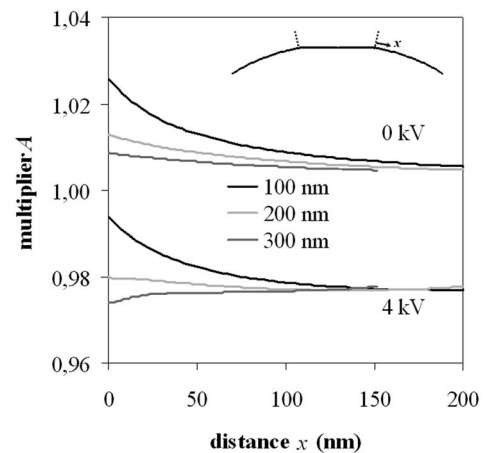


FIG. 7. Variation in multiplier  $A$  [proportional to adatom equilibrium concentration, Eq. (9)] along the surface of the emitters in Fig. 5 with  $p = 0.05 \text{ e}\text{\AA}$ ,  $\beta = 0.2 \text{ eV}/\text{\AA}$ , and  $T = 1800 \text{ K}$ .

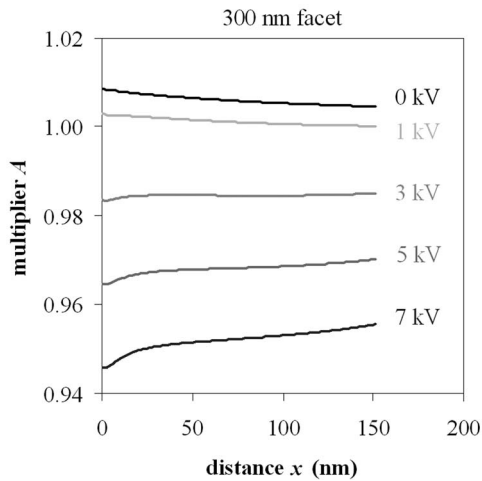


FIG. 8. Variation in multiplier  $A$  [Eq. (9)] along the surface of the emitter with a facet 300 nm in diameter (Fig. 5) as a function of extraction voltage with  $p=0.05 \text{ e}\text{\AA}$ ,  $\beta=0.2 \text{ eV/\text{\AA}}$ , and  $T=1800 \text{ K}$ .

By applying the extraction voltage, the concentration reduces because the positive dipole moment increases the work to create an adatom. The effect of the voltage is smallest for the tip with the 100 nm facet because the field and field gradient are smallest (Fig. 6). For this facet, the concentration gradient still is such that atom transport is pointing away from the apex, and this is also the case for the 200 nm facet tip. For the tip with the 300 nm facet, however, for which the field and field gradient are strongest, the concentration gradient is reversed. For this tip, the atom transport is expected to be toward the facet. For the chosen material properties and extraction voltage, collapsing rings are thus expected for the 100 and 200 nm facet tips but not for the 300 nm facet tip. From Fig. 7, we conclude that, for a positive dipole moment, the driving force for decay through collapsing rings due to step radius differences will be reduced and can even be reversed when the potential difference between the emitter and extractor is applied. We think that this applies to the experimental “ring-stopping field” results.

Whether or not a given emitter tip is expected to collapse and cause probe instabilities for a chosen extraction voltage depends on the exact emitter geometry and the field distribution along its surface. From Eq. (9) the condition for collapse prevention is

$$\frac{dE(x)}{dx} \geq \frac{\Omega_s \beta}{p} \frac{dr^{-1}(x)}{dx}, \quad (10)$$

which must be valid along all of the stack.

For the tip-end geometries investigated here and the extraction voltage of 4 kV, this is true only for the 300 nm facet tip. The tips with the smaller facets require much larger, impractical extraction voltages (for tip with 200 nm facet  $>7 \text{ kV}$ ): for these tips, a collapse cannot be prevented.

It is noted that for the investigated shapes, no extraction voltage could be found for which  $A$  was constant along the whole tip-end surface and the tip would be fully stable. Figure 8 shows the variation in the multiplier along the surface

of the tip with the 300 nm facet for different extraction voltages. The most stable probe from the emitter is expected for a condition in which the variation in  $A$  is small and the direction of net diffusion is not pointing away from the apex anywhere on the tip end (no collapse). From Figs. 7 and 8, this would be for the tip with the 300 nm facet an extraction voltage between 3 and 4 kV.

To make a good comparison with the experimental ring-stopping field found by Swanson and Schwind,<sup>1</sup> we would have to know the exact shape of the tip end for which the result was obtained. The conversion of their experimental extraction voltage to a ring-stopping facet field was based on finite-difference calculations for a sphere-on-cone geometry, with the sphere truncated by a facet with a diameter of  $0.6r_{\text{tip}}$ . For an emitter with a  $0.5 \mu\text{m}$  tip radius, this gives a facet diameter of 300 nm and a contact angle of  $17^\circ$ . The emitter profile we have taken from the contour on the SEM image is slightly different, and determining a tip radius is not straightforward. We have drawn a circle of  $0.5 \mu\text{m}$  radius in the profile in Fig. 5. The field at the facet center of the tip with the 300 nm facet, for which collapse is not expected, is somewhere between 0.53 and 0.74 V/nm (corresponding to a 3–4 kV extraction voltage), to compare to the experimental ring-stopping field of 0.8 V/nm.<sup>1</sup> It is noted that the position and shape of the curves in Figs. 7 and 8 will change with different estimates of the dipole moment and step line tension and by taking into account step-step interaction and the field dependence of the step properties. Altogether, we believe our results to be in reasonable agreement with the experimental value given by Swanson and Schwind.<sup>1</sup>

## VIII. DISCUSSION

It is noted that the model can only give the momentarily expected direction of diffusion. To calculate the evolution of the tip end, the diffusion equations have to be solved, which requires a few more material properties and an extension of the model to the shanks of the emitter, because we need a boundary condition of zero transport. We do not expect our model [(100) terraces] to hold for the range of crystallographic orientations traversed when going from the tip to the shank. It is unknown if the material transport would lead to a fully stable tip shape.

From Figs. 7 and 8, it can be seen that by applying an extraction voltage, the value of  $A$  can become smaller than 1. A value of 1 is equivalent to the equilibrium concentration on a large terrace with zero field. The electric-field strength decreases with increasing distance from the apex, which implies that for (100) terraces further down the shanks of the emitter, the multiplier value is  $\geq 1$ . By applying an extraction voltage, the concentration difference between the tip area and shank area is thus also changed, which could give net diffusion toward the tip. This suggests that depending on the tip geometry and extraction voltage, the concentration gradient in the tip area can point away from the apex (collapsing rings), while at the same time there is a concentration difference promoting diffusion from the shanks toward the tip (e.g., for 4 kV for the 100–200 nm facet tip in Fig. 7). Long-

term stability of the shape of the emitter therefore seems impossible. This was also found by Dyke *et al.*<sup>21</sup> within the approach of Sec. IV. They calculated that for a field that stops net diffusion in the tip area [ $E_{\text{stop}}$ , Eq. (1)], there is still a difference in surface chemical potential between the shanks and tip.

In the absence of a field, it has been shown within the step-flow model that with every collapse, the new facet at the tip end is larger than the previous.<sup>4</sup> This is still expected for tips with very small facets and contact angles in the presence of a field: the field gradient along the surface is much smaller than the gradient in step curvature. However, assuming that apart from the layers peeling off that the shape is maintained, the field gradient will become stronger with increasing facet size, and for a certain facet size the collapses will stop. We think that this also describes the final stage in the manufacturing process for Schottky emitters: creating the facet at the tip end. This is done by applying an extraction voltage to the spherical tip end. In this process, the emitter will first go through several collapses. However, after some time, the collapsing stops and the characteristic facet forms.<sup>1</sup>

The model is limited to rotationally symmetric tip ends. Schottky emitters that have been operating at higher extraction voltages often display faceted tip ends. The faceting is a result of the increasing anisotropy of the surface tension for different crystallographic orientations with increasing field.<sup>22</sup> For a faceted tip, the end facet will no longer be circular and its edges will match directly to other low-index facets [(110) and/or (112) planes], and the tip-end area can no longer be described with a stack of concentric (100) terraces. When such a tip is heated in the absence of a field or at very low extraction voltages, the faceting will disappear again.

## IX. CONCLUSION

The phenomenon of collapsing rings on Schottky emitters can be explained by step-flow models. Collapsing rings can be prevented with a strong enough field gradient along the emitter surface. This can be achieved by applying high enough extraction voltages. Whether a given emitter for given operation conditions is likely to collapse can be predicted provided its exact shape and the relevant material properties are known.

- <sup>1</sup>L. W. Swanson and G. A. Schwind, in *Handbook of Charged Particle Optics*, edited by J. Orloff (CRC, New York, 1997), Chap. 2, p. 77.
- <sup>2</sup>J. K. Trolan, J. P. Barbour, E. E. Martin, and W. P. Dyke, *Phys. Rev.* **100**, 1646 (1955).
- <sup>3</sup>J. P. Barbour, F. M. Charbonnier, W. W. Dolan, W. P. Dyke, E. E. Martin, and J. K. Trolan, *Phys. Rev.* **117**, 1452 (1960).
- <sup>4</sup>N. Israeli and D. Kandel, *Phys. Rev. B* **60**, 5946 (1999).
- <sup>5</sup>M. Giesen, G. Beltramo, S. Dieluweit, J. Müller, H. Ibach, and W. Schmickler, *Surf. Sci.* **595**, 127 (2005).
- <sup>6</sup>P. C. Bettler and G. Barnes, *Surf. Sci.* **10**, 165 (1968).
- <sup>7</sup>C. Herring, in *The Physics of Powder Metallurgy*, edited by W. E. Kingston (McGraw-Hill, New York, 1951), Chap. 8, p. 143.
- <sup>8</sup>F. A. Nichols and W. W. Mullins, *J. Appl. Phys.* **36**, 1826 (1965).
- <sup>9</sup>H. P. Bonzel, *Phys. Rep.* **385**, 1 (2003).
- <sup>10</sup>S. Tanaka, N. C. Bartelt, C. C. Umbach, R. M. Tromp, and J. M. Blakely, *Phys. Rev. Lett.* **78**, 3342 (1997).
- <sup>11</sup>P. C. Bettler, D. H. Bennum, and C. M. Case, *Surf. Sci.* **44**, 360 (1974).
- <sup>12</sup>M. Degawa, K. Thürmer, and E. D. Williams, *Jpn. J. Appl. Phys., Part 1* **45**, 2070 (2006).
- <sup>13</sup>M. Giesen, *Prog. Surf. Sci.* **68**, 1 (2001).
- <sup>14</sup>N. Hirai, K. Watanabe, and S. Hara, *Surf. Sci.* **431**, 568 (2001).
- <sup>15</sup>M. Horn-Von Hoegen, F.-J. Meyer zu Heringdorf, D. Kähler, T. Schmidt, and E. Bauer, *Thin Solid Films* **336**, 16 (1998).
- <sup>16</sup>J. Müller and H. Ibach, *Phys. Rev. B* **74**, 085408 (2006).
- <sup>17</sup>H. Ibach and W. Schmickler, *Phys. Rev. Lett.* **91**, 016106 (2003).
- <sup>18</sup>CPO2D, CPO programs (<http://www.electronoptics.com>).
- <sup>19</sup>K. Besocke and H. Wagner, *Phys. Rev. B* **8**, 4597 (1973).
- <sup>20</sup>W. Xu, J. B. Adams, and T. L. Einstein, *Phys. Rev. B* **54**, 2910 (1994).
- <sup>21</sup>W. P. Dyke, F. M. Charbonnier, R. W. Strayer, R. L. Floyd, J. P. Barbour, and J. K. Trolan, *J. Appl. Phys.* **31**, 790 (1960).
- <sup>22</sup>S. Fujita and H. Shimoyama, *Phys. Rev. B* **75**, 235431 (2007).